HHS Public Access

Author manuscript

Cancer Treat Res Commun. Author manuscript; available in PMC 2021 May 17.

Published in final edited form as:

Cancer Treat Res Commun. 2021 ; 27: 100315. doi:10.1016/j.ctarc.2021.100315.

The impact of initial tumor microenvironment on imaging phenotype

Tavarekere N Nagaraja[a,*,1], **Ana C deCarvalho**[a,1], **Stephen L Brown**[c,j], **Brent Griffith**[d], **Katelynn Farmer**[i], **Susan Irtenkauf**[a], **Laura Hasselbach**[a], **Abir Mukherjee**[e], **Seamus Bartlett**[k,a], **O. Grahm Valadie**[j], **Glauber Cabral**[b], **Robert A Knight**[b,g], **Ian Y Lee**[a], **George W Divine**[f], **James R Ewing**[a,b,g,h]

[a]Department of Neurosurgery, Henry Ford Hospital, Detroit, MI

[b]Department of Neurology, Henry Ford Hospital, Detroit, MI, United States

[c]Department of Radiation Oncology, Henry Ford Hospital, Detroit, MI, United States

[d]Department of Radiology, Henry Ford Hospital, Detroit, MI, United States

[e]Department of Pathology, Henry Ford Hospital, Detroit, MI, United States

[f]Department of Public Health, Henry Ford Hospital, Detroit, MI, United States

[g]Department of Physics, Oakland University, Rochester, MI, United States

[h]Department of Neurology, Wayne State University, Detroit, MI, United States

[i]Department of Biomedical Engineering, Wayne State University, Detroit, MI, United States

[j]Department of Radiation Oncology, Wayne State University, Detroit, MI, United States

[k]School of Medicine, Wayne State University, Detroit, MI, United States

[*]Corresponding author at: Department of Neurosurgery, Room E&R-3096, Henry Ford Hospital, 2799 West Grand Blvd., Detroit, MI 48202-2689, USA. tnagara1@hfhs.org (T.N. Nagaraja).

[1] These authors contributed equally to the work.

Author contribution section

Tavarekere N. Nagaraja performed the studies, analyzed the data and prepared the original draft of the paper. Ana C. deCarvalho provided neurospheres as well as expert advice for their implantation, supervised the RPPA analysis and edited the paper. Stephen L. Brown prepared the neurospheres for implantations, did data analysis, acquired funding and reviewed and edited the paper. Brent Griffith analyzed and scored the contrast-enhancement patterns of the different PDOX tumors derived in the study, helped compare them to their corresponding human MR images and edited the paper. Katelynn Farmer analyzed the MRI data and derived the MR quantitative parameter values. Susan Irtenkauf took part in tumor implantations, data management, tissue preparation for histopathology and edited the paper. Laura Hasselbach prepared the neurosphered for implantations, took part in tumor implantations and performed tissue microdissections for RPPA analysis. Abir Mukherjee evaluated the H&E and MHC histologies. Seamus Bartlett did histology image acquisition and analysis. O. Grahm Valadie performed MRI data analysis and edited the paper. Glauber Cabral performed MR imaging and edited the paper. Robert A. Knight assisted in MRI data curation and analysis and edited the paper. Ian Y. Lee provided expert advice on human biopsy tissues, evaluated the human MRI images used and edited the paper. George W. Divine performed statistical analysis of the data and edited the paper. James R. Ewing conceptualized and supervised the study, provided expert advice, acquired funding and also reviewed and edited the paper.

Declaration of Competing Interest

The authors declare that they have no known competing financial interests or personal relationships that could have appeared to influence the work reported in this paper. The authors declare the following financial interests/personal relationships which may be considered as potential competing interests: Dr. Ian Y. Lee has consulting agreements with Medtronic, Inc., Minneapolis, MN and Monteris Medical, Inc., Plymouth, MN. All the other authors declare no competing financial or personal relationships that could have appeared to influence the work reported in this paper.

Supplementary materials

Supplementary material associated with this article can be found, in the online version, at doi:10.1016/j.ctarc.2021.100315.

Abstract

Models of human cancer, to be useful, must replicate human disease with high fidelity. Our focus in this study is rat xenograft brain tumors as a model of human embedded cerebral tumors. A distinguishing signature of such tumors in humans, that of contrast-enhancement on imaging, is often not present when the human cells grow in rodents, despite the xenografts having nearly identical DNA signatures to the original tumor specimen. Although contrast enhancement was uniformly evident in all the human tumors from which the xenografts' cells were derived, we show that long-term contrast enhancement in the model tumors may be determined conditionally by the tumor microenvironment at the time of cell implantation. We demonstrate this phenomenon in one of two patient-derived orthotopic xenograft (PDOX) models using cancer stem-like cell (CSC)-enriched neurospheres from human tumor resection specimens, transplanted to groups of immune-compromised rats in the presence or absence of a collagen/fibrin scaffolding matrix, Matrigel. The rats were imaged by dynamic contrast-enhanced magnetic resonance imaging (DCE-MRI) and their brains were examined by histopathology. Targeted proteomics of the PDOX tumor specimens grown from CSC implanted with and without Matrigel showed that while the levels of the majority of proteins and post-translational modifications were comparable between contrast-enhancing and non-enhancing tumors, phosphorylation of Fox038 showed a differential expression. The results suggest key proteins determine contrast enhancement and suggest a path toward the development of better animal models of human glioma. Future work is needed to elucidate fully the molecular determinants of contrast-enhancement.

Keywords

Contrast enhancement; Glioblastoma; Matrigel; MRI; Neurospheres; PDOX models; Rat

Introduction

Glioblastoma (GBM), the most common of high grade gliomas (HGGs), presents a deadly puzzle for medicine. Glioblastoma is treated with maximal surgical removal, followed by radiation therapy (RT) and DNA-alkylating agent temozolomide (TMZ) [1]. Despite this aggressive multi-modality treatment, most patients show treatment refractory relapse within months, with a dismal 2 year survival rate of 15.2% [2]. Even with the best care, *i.e.* surgery, radiotherapy and temozolomide, GBM is incurable and quickly fatal, with a mean time from diagnosis to death of about 15 months [3, 4]. This dismal therapeutic landscape is made even darker by a dearth of truly representative animal models of GBM [5–7]. Huszthy et al. [6] noted, "… there are a vast number of reports showing the therapeutic efficacy of novel treatment modalities in various animal models, yet when these are further evaluated in the clinic, they fail in phase II/III clinical trials." In the intervening years, little has changed: Aldape et al., in a 2019 review [5], described seven challenges for the scientific community, one of which is to develop preclinical models of human cancers. In studying this malignant disease, animal models are a necessary first step in testing putative therapies; in order to be useful, they should recapitulate the salient pathophysiology of the disease.

Neurosphere cultures derived from tumor biopsy and grown in serum-free media have been shown to preserve the genomic features of the original tumor, and form patient-derived

orthotopic xenograft (PDOX) tumors in immunocompromised mice [6–15]. Because they so closely echo the genotypes of their parent tumors [8, 16, 17], PDOXs can be considered to be the most representative and important tool to study treatments intended to interfere with the complex genetic alterations involved in *in vivo* tumorigenicity and progression of GBM [14, 15, 18, 19]. However, these best current models of GBM have an unrecognized flaw. We [20] and others [6] have observed that PDOX's mimicry of the human disease is impaired, in that instances of magnetic resonance imaging (MRI)-visible blood-brain barrier (BBB) breakdown are rare. In fact, PDOXs are typically infiltrative [15] and generally do not exhibit MRI contrast enhancement, despite the clinical MRI displaying florid central enhancement in the main tumor mass from which these models were derived.

Two mutually exclusive cellular behaviors have been observed in glioma tumors - slow moving proliferative cells ('grow'), or mainly infiltrative migratory cells ('go') with lower proliferation rate [21]. The enhancing mass of the tumor (the 'grow' population) is characterized by an incompetent vasculature, central hypoxia, pseudopalisading necrosis, increased interstitial fluid pressure, and peri-tumoral flux [22, 23]. This physiology is substantially different from the physiology of the 'go' population, where proliferation is suppressed and resistance to apoptosis and drug therapy is increased [21]. Thus, PDOXs without BBB breakdown model the infiltrative cell population, but not the enhancing proliferative tumor mass, and therefore represent an incomplete model of the human pathology from which they were derived. This partial fidelity to the original pathology has potential to compromise the assessment of trial therapies, and of combination therapies, regardless of dependency on BBB breakdown for delivery. Interestingly, glioma stem cells can adopt invasive or proliferative phenotypes [24], accumulating in perivascular niches and hypoxic regions [25].

The lack of phenotypic recapitulation of human tumors is suggested to lie in the interaction between the implanted tumor cells and host stroma [26]. We hypothesized that manipulation of the tumor stromal composition by addition of Matrigel, a basement membrane preparation, would produce a consistent BBB breakdown in murine PDOX models of GBM. To test this hypothesis, reconstituted basement membrane derived from Engelbreth-Holm-Swarm (EHS) mouse sarcoma Matrigel [27, 28], with high and low growth factor content, was used to manipulate the brain microenvironment during patient-derived cancer stem-like cell (CSC) implantation and the radiological presentations of the resultant tumors were examined by DCE-MRI.

Materials and methods

Athymic, immune-compromised female RNU/RNU rats were acquired from Charles River, Frederick, MD. Matrigel Matrix-Growth factor reduced and Matrigel Basement Membrane Matrix-High concentration were purchased from Corning and BD Biosciences, respectively. All other reagents and labware used were of analytical grade.

Patient-derived neurosphere cell lines

Following an approved Institutional Review Board protocol, resected brain tumor specimens were collected and processed at Hermelin Brain Tumor Center, Henry Ford Hospital, with

written consent from patients. Tumors were pathologically graded according to the WHO criteria. GBM specimens were dissociated and cultured in serum-free neurosphere medium to enrich CSC [9]. HF2303 and HF3016 CSC lines were derived from newly diagnosed tumors from two glioblastoma patients in which MRI studies showed typical ring-enhancing lesions. These neurosphere lines were tumorigenic, and molecular profiling show that genomic abnormalities present in the parental tumors were preserved in these models [17, 29, 30].

Orthotopic rat xenografts

For intracranial implantation, neurospheres were dissociated to single cells in Dulbecco's phosphate buffered saline (PBS) following published methods [9, 11]. A 10 μl volume containing 3×10^5 cells was used for implantation in each rat. The cells were suspended in 10 μl sterile PBS (M0), 5 μl PBS+5 μl Matrigel with reduced growth factors (M−) or 5 μl PBS+5 μl Matrigel with high growth factors (*M*+). Thirty-two female, athymic, immune-compromised rats were randomly distributed between the 3 subgroups, M0, M− and *M*+. Following published methods [31, 32], one of the two neurosphere cell lines was implanted into the right hemisphere in these rats under a protocol approved by the Institutional Animal Care and Use Committee. Briefly, animals were anesthetized with isoflurane (4% for induction, 1.5% for maintenance, balance N_2O:O_2 = 2:1). Under aseptic conditions, the scalp was swabbed with Betadine and alcohol, the eyes coated with Lacri-lube (Allergan Inc., Madison, New Jersey) and the head immobilized in a rat stereotactic device (Kopf, Cayunga, California). A 1 cm incision was made 2 mm right of the midline and the skull exposed and a burr hole drilled 3.5 mm to the right of bregma without penetrating the dura mater. A 10 μl Hamilton syringe with a 26 gauge needle containing the tumor neurosphere cells was lowered to a depth of 3.0 mm and then raised back to a depth of 2.5 mm. Cells were then injected at a rate of 0.5 μl/10 s until the entire volume was injected. The needle was gently withdrawn, the burr hole sealed with sterile bone wax and the scalp sutured with sterile silk sutures. The rats were observed until complete recovery and then placed back in their home cages.

Imaging

All studies used a Varian/Magnex (Santa Clara, California), 7 Tesla, 20 cm bore magnet with a Bruker console running Paravision 6.0 software. Gradient maximum strengths and rise times were 250 mT/m and 120 μs. All MRI image sets were acquired with a 32×32 mm^2 FOV. Transmit and receive coils included a Bruker Quadrature Birdcage (transmit) and 4-channel phased-array surface coil receiver (Rapid MR International, Columbus OH). T1-weighted images (T1WIs) were acquired pre- and post-contrast (Magnevist, 0.25 mmol/kg) with the following parameters: matrix: 256 × 192, 27 slices, 0.4 mm thickness, 0.1 mm gap, number of echoes (NE) = 1, number of averages (NA) = 4, TE/TR = 16/800 ms.

A complete set of MRI (T1 and T2) and DCE-MRI parameters (plasma distribution volume, v_p; blood-to-brain forward volume transfer constant, K^{trans}; interstitial volume fraction, v_e; V_D, extracellular distribution volume) for the MR contrast agent (CA) Magnevist (gadopentetate dimeglumine; Bayer Healthcare, Wayne, New Jersey) were acquired using published methods [31, 33]. A unique feature in the DCE-MRI analysis was the use of a

model selection paradigm, which attempted to best balance variance and bias in the estimation of model parameters, and thus stabilize estimates of cerebral physiology produced by DCE-MRI [34].

Histopathology and reverse phase protein array (RPPA) assays

Rats were euthanized by isoflurane overdose, followed by decapitation. Whole brains were quickly removed and placed in rat brain matrix. With the implantation needle entry as the center, 2 mm thick, coronal slices were cut anterior and posterior to the center to generate frozen and formaldehyde fixed, paraffin embedded (FFPE) tissues. Slices for frozen sections were placed on cork circles and were covered in OCT freezing medium prior to flash freezing in 2-methylbutane cooled to —40 °C with dry ice. Slices for FFPE were placed in mesh cassettes and immersion fixed in formaldehyde for later paraffin embedding. Five μm thick sections from the FFPE slices were deparaffinized and processed through a graded alcohol series for hematoxylin and eosin (H&E) staining. Additional 5 μm thick sections underwent a 15 min incubation in pH 6.0 citric acid buffer for antigen retrieval, followed by incubation in Rodent Block M (Biocare Medical, Pacheco, California) for 20 min. They were then incubated with human marker major histocompatibility complex I (MHC; ab52922, Abcam, Cambridge, UK), 1:1000 for 60 min. After primary antibody incubation, slides were incubated for 30 min in Rabbit on Rodent Polymer (Biocare Medical, Pacheco, California) and for 4 min in Betazoid DAB (Biocare Medical, Pacheco, California). Images were captured using a Nikon E800M microscope and DXM1200C digital camera with Image Pro-Plus software (Media Cybernetics, Rockville, MD). Stained sections were examined for tumor location from both H&E and MHC stained specimens.

RPPA

The flash frozen rat brain tissue blocks were stored in a —80 °C freezer until processed for RPPA. One 5 μm section was cut from each slice and stained with H&E to localize the tumor boundaries to aid in dissecting out the tumor tissue. With reference to this staining, tumor tissue was macrodissected, weighed and placed in 5 ml tube on ice. Freshly prepared lysis buffer was added to the tube at a ratio of 40 mg tumor/ml buffer. The tumor tissue was homogenized in the tube on ice for 8 s and then the tubes were centrifuged at 4 °C, 14,000 RPM for 10 min. The supernatants were transferred to another set of microcentrifuge tubes and their protein concentrations were measured and the buffer volume was adjusted to 1.5 μg protein/ml. The lysates were then mixed in 3:1 ratio with sample buffer with 4X sodium dodecyl sulfate, but without bromophenol blue, boiled for 5 min and stored at —80 °C until shipped to MD Anderson Cancer Center for analysis. Brain tissue samples from two rats with no tumor implantation were included as controls.

Data analysis

Parameter maps for T2, T1 pre- and post-contrast were made using published procedures [32, 35]. The analysis of DCE-MRI data followed established procedures [34], with a model selection paradigm centered around the multi-parameter Patlak Plot, and producing, at most, non-biased estimates of the forward vascular transfer constant, K^{trans}, the extravascular, extracellular volume fraction v_e, and the plasma volume, v_p in tissue that had sufficiently permeable vasculature. In general, estimates of K^{trans} and v_e could only be constructed from

those tumors exhibiting true contrast extravasation and could not be constructed in tissues that exhibited post-contrast T1 hyperintensities due to hypercellularity and/or vasodilation.

In addition to the parametric analysis of the DCE-MRI data, the T1 and T2 image sets were examined and graded. A board-certified radiologist blinded to the conditions of the study reviewed all cases and graded each for radiological evidence of BBB breakdown on a scale of 0 to 4, with 0 being no evidence, and 4 being florid enhancement. The radiological images were visually compared to their corresponding histopathology to match tumor location and extent. They were also compared to clinical T2 and post-contrast T1 images after patient de-identification.

Ordinal logistic regression (OLR) modeling and Wilcoxon rank sum tests were used to analyze radiologic BBB breakdown scores. The RPPA data were examined for significant changes in levels of any of the 384 analyzed proteins between tumors from control rats (n = 3) and those implanted with Matrigel (n = 5) using multiple t-tests. Statistical significance was determined using the Holm-Sidak method, with alpha = 0.05.

Results

In 32 animals there were 5 extra-axial masses and 30 intra-axial cerebral tumors. All 5 extra-axial masses enhanced floridly. Two animals with only extra-axial masses were removed from further consideration. The average post-implantation days for all rats in a given neurosphere group at which the tumors were studied were, 84.4 ± 5.8 days for HF2303 PDOX model (mean post-implantation termination time: M0=86.4 days; M−=77.8 days; *M*+=89 days) and 57.2 ± 12.6 days for the HF3016 PDOX model (mean post-implantation termination time: M0=42.7 days; M−=64.3 days; *M*+=64.8 days).

Visually, the two cell lines demonstrated quite different responses to Matrigel, with no subjective difference between *M*+ and M− in either cell line. Typical control HF3016 cell lines (M0) showed little or no T1WI post-Gd enhancement (Fig. 1), and typical *M*+ and M− cell lines showed florid enhancement (Fig. 1). Although HF2303 PDOXs were visible both pre- and post-contrast (Fig. 2), subtraction images showed little post-Gd enhancement under any condition (M0, *M*+, or M−). Fig. 3 summarizes the radiologist's scores via a dot plot; the trends described are clearly reflected therein.

Statistical analysis supported these observations. The OLR model was fit with factors treatment (three levels: M0, *M*+ and M−) and cell line (two levels HF2303 and HF3016). The test for interaction between cell line and *M*+ factor was not significant (p = 0.451). There was also no evidence of a growth factor effect (p = 0.725 for cell line HF2303 and p = 1.0 for cell line HF3016). The Matrigel treated groups with and without growth factor were then combined. After this, the test for interaction between cell line and Matrigel was still not significant (p = 0.195). However, when the Matrigel effect was tested using a Wilcoxon Rank Sum test separately within each cell line, the test was significant for HF3016 (p = 0.004), but not for HF2303 (p = 0.328).

A comparison of MRI parameter maps with histologies showed spatial agreement between the two main tumor masses in both (Figs. 1 and 2). However, the histologies showed

infiltrating tumor tissue along white matter tracts that was not observed on MRI. Such infiltrating tumor regions were more prominently visible on MHC-stained than on H&E-stained images (Fig. 1). The M− and *M*+ cohorts in the HF3016 group could be analyzed for DCE-MRI studies with well-defined regions of vascular breakdown, and amenable for Patlak plot-model selection maps. These quantitative DCE analysis provided information about virtual tumor segmentation in terms of its vascular permeability and contrast agent extravasation for Magnevist (Table 1). A preliminary analysis suggested comparable vascular volumes (v_p), but a trend of increased interstitial spaces in *M*+ rats (elevated v_e and V_D values). However, the differences were not statistically significant (*t*-test).

Apart from the spatial correlation between tumor cells and MRI-visible tumor segments in contrast enhancing PDOXs, the histopathology from the PDOXs exhibited microscopic infiltration that recapitulated human glioma (Fig. 4). Tumor cells, singly and in small clusters that were unaccompanied by contrast enhancement on MRI, were observed to be infiltrating into the surrounding brain tissue. These tumors also showed regions of psueudopalisading necrosis within the main tumor mass.

An interesting feature noted was that extra-axial tumors close to the brain surface, presumably contiguous with pial vasculature, typically showed T1 contrast enhancement independent of its Matrigel status. An example is shown in Fig. 5 wherein two distinct tumor segments are visible, but only the extra-axial tumor segment shows T1 contrast enhancement whereas its intra-axial, embedded segment does not. This phenomenon is also visible in T1 post-pre panels in both figures 1 and 2 wherein extra-axial tumor tissue on cortical surface shows contrast enhancement.

To compare the molecular characteristics of the terminal HF3016 xenograft tumors grown without Matrigel (M0 group, $n = 3$) or with Matrigel (*M*+, M−; $n = 5$) we employed a targeted proteomics approach. The levels of 384 proteins and post-translational modifications, representing key pathways in cancer, were measured in tumor lysates via Reverse Phase Protein Arrays (RPPA). Lysates from two HF3016 preimplant CSC cultures were included (Supplemental Table 1). Using multiple *t*-test with statistical significance determined using the Holm-Sidak method, with alpha = 0.05, we determined that only 3 analytes were significantly different between the M0 and M(+,−) groups (Fig. 6). The phosphorylation of the transcription factor FoxO3 at S318/S321 was significantly decreased in the M(+,−) tumors. The Akt directly phosphorylates these conserved serine residues, leading to FoxO3A nuclear export, thus inhibiting its transcriptional regulation activityOn the other hand, the levels of phospho-S6 (S240/S244), a canonical indicator of mammalian target of rapamycin (mTOR) activity, and of the UV excision repair protein Rad23 homolog A (Rad23A) were significantly increased in the Matrigel group. Prior to implant, HF3016 presented low levels of phospho-S6, phospho-FoxO3A and Rad23A relative to PDOXs.

Discussion

Using two patient-derived neurospheres, this study describes a simple method that shows promise for inducing an intra-axial PDOX brain tumor that presents radiological features of the parent tumor. Such tumors showed a contrast MRI-visible, space occupying tumor mass

with MRI-invisible, infiltrating tumor regions, similar to human GBM. However, the method needs to be tested with other neurosphere cultures and matrix scaffolding preparations to fine-tune the combination to suit given human GBM neurospheres. As a practical matter for preclinical studies, a reliable BBB breakdown in PDOX models represents a significant advance in the assessment of trial therapies because it produces an experimental condition closer to the human pathology of interest. However, as demonstrated herein, the effect of stromal enhancement is cell-line dependent, and the biological correlates that accompany BBB breakdown after stromal enhancement still need to be described, an interesting question in itself. Despite these limitations, note that tumor visualization via T1 contrast-enhancement is the clinical standard that determines the extent of tumor resection in both newly diagnosed and recurrent GBM [36, 37]. An orthotopic animal model that recapitulates this critical feature while also retaining the molecular fingerprints of the patient tumor will be highly valuable in testing new therapies.

Using targeted proteomics to evaluate any lasting effect of Matrigel on molecular composition of the tumors, we showed that the terminal tumors from cells implanted with Matrigel were indistinguishable from those implanted without Matrigel in relation to the levels of the majority of analyzed key proteins and post-translational modifications measured. In the tumors from the Matrigel group we observed a decrease in phosphorylation of FoxO3 at the S318 and S321 residues, suggesting increased nuclear accumulation. FoxO3 is a transcription factor involved in homeostasis regulation in neural stem cells [38]. Interestingly, an increase in phospho-S6, a marker of mTOR activity, was also observed in the Matrigel group.

In neural stem cells, FoxO3 is the major member of the FoxO family. Phosphorylation of FoxO3 via phosphoinositide-3-kinase (PI3K)-AKT results in its binding of protein 14–3–3, and its subsequent exclusion from the nucleus to the cytoplasm, i.e., its inactivation. Once FoxO3 is removed from its nuclear site, its suppression of cell cycling is disabled, which leads to in-situ proliferation [39]. FoxO's are lineage-restricted redundant tumor suppressors [40]. According to Paik et al., FoxO3 also plays a role in angiogenesis, although not exclusively. Complete knockout of FoxO's in mice resulted in a hemangiomic phenotype, mainly due to FoxO1 knockout, but also related to FoxO3 knockout in endothelial cell populations [40]. Its relevance to the PDOX phenomena needs further studies because the vasculature recruited by the tumor cells is probably murine vasculature with a full complement of FoxO's.

We note that there are some limitations to these data with regards to known inconsistencies in Matrigel preparations. This is also evident in the present data where the two Matrigel preparations gave rise to slightly different tumors. Use of M− resulted in tumors with slightly lower K^{trans}, and v_e and V_D suggesting more tumor cell density [35] than in *M*+ tumors. The stated compositions of the two Matrigel matrix preparations were similar, *i.e.*, laminin as a major component, collagen IV, heparan sulfate proteoglycans, entactin/nidogen, and several growth factors. However, the proportions of these moieties and the growth factors could be different between the two leading to slightly different tumor subtypes *in vivo*. A tightly controlled Matrigel composition can overcome this limitation which can then be tested with other GBM neurosphere cell lines to generate PDOX models. Also, although

no BBB breakdown was observed in rats after Matrigel injection (Supplemental data), we concede that more subtle parenchymal effects than a disturbance of the BBB may have occurred in the vicinity of the injection.

While no animal model is completely representative of human disease in all its complexity, the establishment of tumors in immune-deficient animals by xenografting human tumor material, mostly in the form of cell lines and biopsies, has been invaluable in the search for mechanisms that determine tumor growth and progression [11, 12, 14, 15, 26]. Xenograft models include human biopsy spheroid xenograft, human glioma cell monolayers grown in serum-containing media and human glioma-derived neurospheres grown in serum-free neurobasal media. Xenograft tumors from established 2D serum-cultured glioma cells lines are fast growing, reproducible, and generate a BBB breakdown, but the tumors deviate in genotypic and phenotypic characteristics (typically reduced invasiveness) from the original patient tumor [6, 26]. Further, developing models from low grade gliomas has proven difficult with this approach. In contrast, neurospheres grown in serum-free media more closely reiterate the molecular makeup of the original patient tumor, with molecular profiles being more stable over time [6, 8, 9, 11, 26]. This approach is also suitable for low grade gliomas. Neurospheres grown as PDOXs are now considered as the most representative and important tool to study *in vivo* tumorigenicity and progression of GBM [14, 15, 18, 41].

As we and others have noted [5, 6], multiple experimental therapies effective in animal models have failed in clinical trials [42, 43]. The success of treating model brain tumors in rodents and the failure in human GBM in a clinical setting is attributed to such factors as the tumor models: (1) do not reflect the biological properties of the patient tumors, and (2) they do not reflect the cellular and molecular heterogeneity of human tumors. The inability of current preclinical systems to mimic the biology of human GBM *in situ* is increasingly cited as a key cause of low success rates for translation of drug discovery efforts to the clinic [44]. Therefore, there is an urgent need for more reliable *in vivo* models in order to facilitate the elucidation of pathophysiology and for testing new drugs and therapies. In this work, we present compelling evidence that a relatively minor manipulation of the extracellular matrix (ECM) during tumor implantation can result in PDOX tumors that are radiologically similar to the human tumors they were derived from.

Matrigel is used to provide a stiff matrix for tumor cells' development into three dimensional and organoid tumor models [45–47]. Matrigel has been extensively used for subcutaneous and to a lesser extent orthotopic *in vivo* tumor cell implantation to presumably enhance tumor take rate and growth [48–50]. Although the specific mechanisms leading to tumor growth enhancement by Matrigel are not well understood, it likely involves stimulation of CSC survival and proliferation, as observed by neural progenitor cells implanted in rodent spinal cord and brain [51, 52]. Some protocols recommend mixing tumor cells with low growth factors-Matrigel before initial heterotopic implantation and later heterotopic *in vivo* passaging [53]. Interestingly, this protocol does not recommend the use of Matrigel in intra-cranial implantations [53]. However, other studies have used co-implantation of tumor cells and Matrigel in both heterotopic [53, 54] and orthotopic GBM preparations [55, 56]. Das et al. used a 1:1 mixture of GBM cells and Matrigel for intra-cranial implantations [56], but did not specify the Matrigel type. The orthotopic tumors derived from them and implanted in

mice brains seemed to be continuous with pial distribution and showed hyperintensity. The imaging sequences not being specified and the observed contiguity with pial vasculature, however, make it difficult to determine the extent of T1 contrast enhancement in these tumors [56]. Tsoli et al. generated *in vivo* models of diffuse intrinsic pontine glioma with implantations with and without Matrigel, but reported no specific effects of Matrigel on resultant tumors [55].

One study has reported evidence of nodular tumor growth and a modest correlation in post-contrast enhancement to the human tumor in one of the seven mouse PDOX models studied [57]. The authors concluded that the MRI features of patient-derived xenograft glioma models were different compared with those of the original patient tumors. Nonetheless, generation of PDOX models of GBM consistently recapitulating radiologic features of patient tumors is still not widely reported. It is important to note that some previous attempts have been made to develop rat PDOX models that exhibit both the characteristic GBM phenotypes, *i.e.*, high neovascularization and diffuse infiltration [58–60]. This is deemed necessary since a typical GBM exhibits a solid, angiogenesis-dependent tumor with mass effect as well as infiltrative, vascular co-opting segments and, thus, essential for an experimental tumor to replicate these features [61]. Sakariassen et al. reported developing angiogenesis-dependent tumors from infiltrative tumors after several successive *in vivo* passages in immune-suppressed rats [59]. First generation tumors in this series showed diffuse lesions that occupied most of the implanted hemisphere and just T2 hyperintensity, atypical of patient tumors. After serial *in vivo* passaging for 4–5 generations, the resultant tumors became more vascular and circumscribed with emerging necrotic regions along with T1 contrast enhancement. However, as noted before, the procedures required that GBM spheroids from rat tumors be passaged *in vivo* into the next generation of nude rats. Similar results have been reported by two other groups. Thorsen et al. used spheroids generated from tumor biopsy specimens for initial orthotopic implantation; they reported forming a more typical GBM-like orthotopic tumor with extensive angiogenesis and necrosis from an initially highly infiltrative, non-angiogenic tumor after three serial passages in immune-suppressed rats [60]. It took about six *in vivo* passages in another study to arrive at a similar model [58]. In comparison to these studies, the approach described in the present work will likely result in a representative tumor phenotype from a GBM neurosphere cell line in the first generation of implanted rats, saving time and resources, and minimizing possible clonal selection alterations over serial *in vivo* passaging. Further work with other available human neurosphere lines that are being generated to test precision medicine approach will elucidate the wider applicability of this technique. With the short overall survival for GBM, minimizing the time needed to test a putative therapy in the animal model that most closely resembles the characteristics of human tumor and reflects its response to therapy is critical for overcoming the significant challenges for effective treatment for GBMs.

Supplementary Material

Refer to Web version on PubMed Central for supplementary material.

Acknowledgements

All the authors have read and agree with the contents. The authors thank Lisa Scarpace for help in accessing archival clinical data, and Jun Xu and Andrea Transou for technical assistance. Research reported in this publication was supported by Henry Ford Cancer Institute 'Game on Cancer' Research Fund H10238 (JRE) and National Cancer Institute of the National Institutes of Health under award number R01CA218596 (JRE and SLB). The content is solely the responsibility of the authors and does not necessarily represent the official views of the Henry Ford Cancer Institute and the National Institutes of Health.

Abbreviations

CSC	cancer stem-like cells
DCE-MRI	dynamic contrast-enhanced magnetic resonance imaging
PDOX	patient-derived orthotopic xenograft
HGG	high grade glioma
GBM	glioblastoma
BBB	blood-brain barrier
EHS	Engelbreth-Holm-Swarm
PBS	phosphate buffered saline
T1WI	T1-weighted images
NE	number of echoes
FOV	field of view
DAB	3,3'-Diaminobenzidine
OCT	optimal cutting temperature
RPM	revolutions per minute
T1WI	T1-weighted images
NE	number of echoes
NA	number of averages
CA	contrast agent
RPPA	Reverse Phase Protein Array
FFPE	formaldehyde fixed, paraffin embedded
H&E	hematoxylin and eosin
MHC	major histocompatibility complex
OLR	Ordinal logistic regression

Akt	Protein kinase B
mTOR	mammalian target of rapamycin

References

[1]. Stupp R, Hegi ME, Mason WP, van den Bent MJ, Taphoorn MJ, Janzer RC, Ludwin SK, Allgeier A, Fisher B, Belanger K, Hau P, Brandes AA, Gijtenbeek J, Marosi C, Vecht CJ, Mokhtari K, Wesseling P, Villa S, Eisenhauer E, Gorlia T, Weller M, Lacombe D, Cairncross JG, Mirimanoff RO, Effects of radiotherapy with concomitant and adjuvant temozolomide *versus* radiotherapy alone on survival in glioblastoma in a randomised phase III study: 5-year analysis of the EORTC-NCIC trial, Lancet Oncol 10 (2009) 459–466. [PubMed: 19269895]

[2]. Ostrom QT, Gittleman H, Fulop J, Liu M, Blanda R, Kromer C, Wolinsky Y, Kruchko C, Barnholtz-Sloan JS, CBTRUS statistical report: primary brain and central nervous system tumors diagnosed in the United States in 2008–2012, Neuro-Oncology 17 (4) (2015) iv1–iv62. Suppl. [PubMed: 26511214]

[3]. Stupp R, Mason WP, van den Bent MJ, Weller M, Fisher B, Taphoorn MJB, Belanger K, Brandes AA, Marosi C, Bogdahn U, Curschmann J, Janzer RC, Ludwin SK, Gorlia T, Allgeier A, Lacombe D, Cairncross JG, Eisenhauer E, Mirimanoff RO, European Organisation for Research and treatment of cancer brain tumor and radiotherapy groups, National Cancer Institute of Canada Clinical Trials Group. Radiotherapy plus concomitant and adjuvant temozolomide for glioblastoma, N. Engl. J. Med 352 (2005) 987–996. [PubMed: 15758009]

[4]. Johnson DR, O"Neill BP, Glioblastoma survival in the United States before and during the temozolomide era, J. Neurooncol 107 (2012) 359–364. [PubMed: 22045118]

[5]. Aldape K, Brindle KM, Chesler L, Chopra R, Gajjar A, Gilbert MR, Gottardo N, Gutmann DH, Hargrave D, Holland EC, Jones DTW, Joyce JA, Kearns P, Kieran MW, Mellinghoff IK, Merchant M, Pfister SM, Pollard SM, Ramaswamy V, Rich JN, Robinson GW, Rowitch DH, Sampson JH, Taylor MD, Workman P, Gilbertson RJ, Challenges to curing primary brain tumours, Nat. Rev. Clin. Oncol 16 (2019) 509–520. [PubMed: 30733593]

[6]. Huszthy PC, Daphu I, Niclou SP, Stieber D, Nigro JM, Sakariassen PO, Miletic H, Thorsen F, Bjerkvig R, *In vivo* models of primary brain tumors: pitfalls and perspectives, Neuro-Oncology 14 (2012) 979–993. [PubMed: 22679124]

[7]. Levin VA, Abrey LE, Heffron TP, Tonge PJ, Dar AC, Weiss WA, Gallo JM, CNS anticancer drug discovery and development: 2016 conference insights, CNS oncology, (2017).

[8]. deCarvalho AC, Nelson K, Lemke N, Lehman NL, Arbab AS, Kalkanis S, Mikkelsen T, Gliosarcoma stem cells undergo glial and mesenchymal differentiation *in vivo*, Stem Cells 28 (2010) 181–190. [PubMed: 19937755]

[9]. Hasselbach LA, Irtenkauf SM, Lemke NW, Nelson KK, Berezovsky AD, Carlton ET, Transou AD, Mikkelsen T, deCarvalho AC, Optimization of high grade glioma cell culture from surgical specimens for use in clinically relevant animal models and 3D immunochemistry, J. Cisual. Experiment.: JoVE (2014) e51088.

[10]. Hidalgo M, Patient-derived tumor xenograft models in drug development, Clin. Adv. Hematol. Oncol.: H&O 15 (2017) 844–846. [PubMed: 29200416]

[11]. Irtenkauf SM, Sobiechowski S, Hasselbach LA, Nelson KK, Transou AD, Carlton ET, Mikkelsen T, deCarvalho AC, Optimization of glioblastoma mouse orthotopic xenograft models for translational research, Comp. Med 67 (2017) 300–314. [PubMed: 28830577]

[12]. Aparicio S, Hidalgo M, Kung AL, Examining the utility of patient-derived xenograft mouse models, Nat. Rev. Cancer 15 (2015) 311–316. [PubMed: 25907221]

[13]. Calvo E, Soria JC, Ma WW, Wang T, Bahleda R, Tolcher AW, Gernhardt D, O'Connell J, Millham R, Giri N, Wick MJ, Adjei AA, Hidalgo M, A phase I clinical trial and independent patient-derived xenograft study of combined targeted treatment with Dacomitinib and Figitumumab in advanced solid tumors, Clin. Cancer Res 23 (2017) 1177–1185. [PubMed: 27733479]

[14]. Joo KM, Kim J, Jin J, Kim M, Seol HJ, Muradov J, Yang H, Choi YL, Park WY, Kong DS, Lee JI, Ko YH, Woo HG, Lee J, Kim S, Nam DH, Patient-specific orthotopic glioblastoma xenograft models recapitulate the histopathology and biology of human glioblastomas *in situ*, Cell Rep 3 (2013) 260–273. [PubMed: 23333277]

[15]. Ji X, Chen S, Guo Y, Li W, Qi X, Yang H, Xiao S, Fang G, Hu J, Wen C, Liu H, Han Z, Deng G, Yang Q, Yang X, Xu Y, Peng Z, Li F, Cai N, Li G, Huang R, Establishment and evaluation of four different types of patient-derived xenograft models, Cancer Cell Int 17 (2017) 122. [PubMed: 29296105]

[16]. Vescovi AL, Galli R, Reynolds BA, Brain tumour stem cells, Nat. Rev. Cancer 6 (2006) 425–436. [PubMed: 16723989]

[17]. deCarvalho AC, Kim H, Poisson LM, Winn ME, Mueller C, Cherba D, Koeman J, Seth S, Protopopov A, Felicella M, Zheng S, Multani A, Jiang Y, Zhang J, Nam DH, Petricoin EF, Chin L, Mikkelsen T, Verhaak RGW, Discordant inheritance of chromosomal and extrachromosomal DNA elements contributes to dynamic disease evolution in glioblastoma, Nat Genet 50 (2018) 708–717. [PubMed: 29686388]

[18]. Izumchenko E, Paz K, Ciznadija D, Sloma I, Katz A, Vasquez-Dunddel D, Ben-Zvi I, Stebbing J, McGuire W, Harris W, Maki R, Gaya A, Bedi A, Zacharoulis S, Ravi R, Wexler LH, Hoque MO, Rodriguez-Galindo C, Pass H, Peled N, Davies A, Morris R, Hidalgo M, Sidransky D, Patient-derived xenografts effectively capture responses to oncology therapy in a heterogeneous cohort of patients with solid tumors, Annal. Oncol 28 (2017) 2595–2605.

[19]. da Hora CC, Schweiger MW, Wurdinger T, Tannous BA, Patient-derived glioma models: from patients to dish to animals, Cells 8 (2019).

[20]. Ewing JR, deCarvalho A, Griffith B, Brown SL, Divine G, Irtenkauf S, Knight RA, Lee IY, Panda S, Cabral G, Nagaraja TN, The Initial Tumor Microenvironment in Cerebral Patient-Derived Glioma Xenografts Affects Their Phenotypical Presentation, International Society for Magnetic Resonance in Medicine, Montreal, Quebec, Canada, 2019.

[21]. Giese A, Bjerkvig R, Berens ME, Westphal M, Cost of migration: invasion of malignant gliomas and implications for treatment, J Clin Oncol 21 (2003) 1624–1636. [PubMed: 12697889]

[22]. Schiffer D, Annovazzi L, Casalone C, Corona C, Mellai M, Glioblastoma: Microenvironment and Niche Concept, Cancers 11 (2018) e1. [PubMed: 30577459]

[23]. Ewing JR, Nagaraja TN, Aryal MP, Keenan KA, Elmghirbi R, Bagher-Ebadian H, Panda S, Lu M, Mikkelsen T, Cabral G, Brown SL, Peritumoral tissue compression is predictive of exudate flux in a rat model of cerebral tumor: an MRI study in an embedded tumor, NMR Biomed 28 (2015) 1557–1569. [PubMed: 26423316]

[24]. Mehta S, Lo Cascio C, Developmentally regulated signaling pathways in glioma invasion, Cellul. Mol. Life Sci.: CMLS 75 (2018) 385–402.

[25]. Calabrese C, Poppleton H, Kocak M, Hogg TL, Fuller C, Hamner B, Oh EY, Gaber MW, Finklestein D, Allen M, Frank A, Bayazitov IT, Zakharenko SS, Gajjar A, Davidoff A, Gilbertson RJ, A perivascular niche for brain tumor stem cells, Cancer Cell 11 (2007) 69–82. [PubMed: 17222791]

[26]. Hidalgo M, Amant F, Biankin AV, Budinska E, Byrne AT, Caldas C, Clarke RB, de Jong S, Jonkers J, Maelandsmo GM, Roman-Roman S, Seoane J, Trusolino L, Villanueva A, Patient-derived xenograft models: an emerging platform for translational cancer research, Cancer Discov 4 (2014) 998–1013. [PubMed: 25185190]

[27]. Benton G, Arnaoutova I, George J, Kleinman HK, Koblinski J, Matrigel: from discovery and ECM mimicry to assays and models for cancer research, Adv. Drug Deliv. Rev 79–80 (2014) 3–18.

[28]. Kleinman HK, Martin GR, Matrigel: basement membrane matrix with biological activity, Semin. Cancer Biol 15 (2005) 378–386. [PubMed: 15975825]

[29]. Berezovsky AD, Poisson LM, Cherba D, Webb CP, Transou AD, Lemke NW, Hong X, Hasselbach LA, Irtenkauf SM, Mikkelsen T, deCarvalho AC, Sox2 promotes malignancy in glioblastoma by regulating plasticity and astrocytic differentiation, Neoplasia 16 (2014) 193–206, 206.e119–125. [PubMed: 24726753]

[30]. Ye LF, Reznik E, Korn JM, Lin F, Yang G, Malesky K, Gao H, Loo A, Pagliarini R, Mikkelsen T, Lo DC, deCarvalho AC, Stockwell BR, Patient-derived glioblastoma cultures as a tool for small-molecule drug discovery, Oncotarget 11 (2020) 443–451. [PubMed: 32064048]

[31]. Elmghirbi R, Nagaraja TN, Brown SL, Keenan KA, Panda S, Cabral G, Bagher-Ebadian H, Lee I, Ewing JR, Toward a noninvasive estimate of interstitial fluid Ppressure by dynamic contrast-enhanced magnetic resonance imaging in a rat model of cerebral tumor, Magn. Reson. Med 00 (2018) 1–13.

[32]. Elmghirbi R, Nagaraja TN, Brown SL, Panda S, Aryal MP, Keenan KA, Bagher-Ebadian H, Cabral G, Ewing JR, Acute temporal changes of MRI-Tracked tumor vascular parameters after combined anti-angiogenic and radiation treatments in a rat glioma model: identifying signatures of synergism, Radiat. Res 187 (2017) 79–88. [PubMed: 28001908]

[33]. Brown SL, Nagaraja TN, Aryal MP, Panda S, Cabral G, Keenan KA, Elmghirbi R, Mikkelsen T, Hearshen D, Knight RA, Wen N, Kim JH, Ewing JR, MRI-tracked tumor vascular changes in the hours after single-fraction irradiation, Radiat. Res 183 (2015) 713–721. [PubMed: 26010711]

[34]. Ewing JR, Bagher-Ebadian H, Model selection in measures of vascular parameters using dynamic contrast-enhanced MRI: experimental and clinical applications, NMR Biomed 26 (2013) 1028–1041. [PubMed: 23881857]

[35]. Aryal MP, Nagaraja TN, Keenan KA, Bagher-Ebadian H, Panda S, Brown SL, Cabral G, Fenstermacher JD, Ewing JR, Dynamic contrast enhanced MRI parameters and tumor cellularity in a rat model of cerebral glioma at 7 T, Magnetic Resonance Med 71 (2014) 2206–2214.

[36]. Serventi J, Behr J, Surgery and evidence-based treatments in patients with newly diagnosed high-grade glioma, Semin. Oncol. Nurs 34 (2018) 443–453. [PubMed: 30409553]

[37]. Suchorska B, Weller M, Tabatabai G, Senft C, Hau P, Sabel MC, Herrlinger U, Ketter R, Schlegel U, Marosi C, Reifenberger G, Wick W, Tonn JC, Wirsching HG, Complete resection of contrast-enhancing tumor volume is associated with improved survival in recurrent glioblastoma-results from the DIRECTOR trial, Neuro-Oncol 18 (2016) 549–556. [PubMed: 26823503]

[38]. Renault VM, Rafalski VA, Morgan AA, Salih DA, Brett JO, Webb AE, Villeda SA, Thekkat PU, Guillerey C, Denko NC, Palmer TD, Butte AJ, Brunet A, FoxO3 regulates neural stem cell homeostasis, Cell Stem Cell 5 (2009) 527–539. [PubMed: 19896443]

[39]. Morris BJ, Willcox DC, Donlon TA, Willcox BJ, FOXO3: a Major Gene for Human Longevity–A Mini-Review, Gerontology 61 (2015) 515–525. [PubMed: 25832544]

[40]. Paik JH, Kollipara R, Chu G, Ji H, Xiao Y, Ding Z, Miao L, Tothova Z, Horner JW, Carrasco DR, Jiang S, Gilliland DG, Chin L, Wong WH, Castrillon DH, DePinho RA, FoxOs are lineage-restricted redundant tumor suppressors and regulate endothelial cell homeostasis, Cell 128 (2007) 309–323. [PubMed: 17254969]

[41]. Persano L, Rampazzo E, Basso G, Viola G, Glioblastoma cancer stem cells: role of the microenvironment and therapeutic targeting, Biochem. Pharmacol 85 (2013) 612–622. [PubMed: 23063412]

[42]. Agnihotri S, Burrell KE, Wolf A, Jalali S, Hawkins C, Rutka JT, Zadeh G, Glioblastoma, a brief review of history, molecular genetics, animal models and novel therapeutic strategies, Arch. Immunol. Ther. Exp. (Warsz.) 61 (2013) 25–41. [PubMed: 23224339]

[43]. Levin VA, Tonge PJ, Gallo JM, Birtwistle MR, Dar AC, Iavarone A, Paddison PJ, Heffron TP, Elmquist WF, Lachowicz JE, Johnson TW, White FM, Sul J, Smith QR, Shen W, Sarkaria JN, Samala R, Wen PY, Berry DA, Petter RC, CNS anticancer drug discovery and development conference white paper, Neuro-Oncol 17 (6) (2015) vi1–v26. Suppl. [PubMed: 26403167]

[44]. Ellis HP, Greenslade M, Powell B, Spiteri I, Sottoriva A, Kurian KM, Current challenges in glioblastoma: intratumour heterogeneity, residual disease, and models to predict disease recurrence, Front. Oncol 5 (2015) 251. [PubMed: 26636033]

[45]. Pauli C, Hopkins BD, Prandi D, Shaw R, Fedrizzi T, Sboner A, Sailer V, Augello M, Puca L, Rosati R, McNary TJ, Churakova Y, Cheung C, Triscott J, Pisapia D, Rao R, Mosquera JM, Robinson B, Faltas BM, Emerling BE, Gadi VK, Bernard B, Elemento O, Beltran H, Demichelis F, Kemp CJ, Grandori C, Cantley LC, Rubin MA, Personalized In Vitro and In Vivo cancer models to guide precision medicine, Cancer Discov 7 (2017) 462–477. [PubMed: 28331002]

[46]. Heffernan JM, Sirianni RW, Modeling microenvironmental regulation of glioblastoma stem cells: a biomaterials perspective, Front. Mater 5 (2018) 7.

[47]. Wolf KJ, Chen J, Coombes JD, Aghi MK, Kumar S, Dissecting and rebuilding the glioblastoma microenvironment with engineered materials, Nature Rev. Mater, 4(2019) 651–668. [PubMed: 32647587]

[48]. Fridman R, Benton G, Aranoutova I, Kleinman HK, Bonfil RD, Increased initiation and growth of tumor cell lines, cancer stem cells and biopsy material in mice using basement membrane matrix protein (Cultrex or Matrigel) co-injection, Nat. Protoc 7 (2012) 1138–1144. [PubMed: 22596226]

[49]. Fridman R, Kibbey MC, Royce LS, Zain M, Sweeney M, Jicha DL, Yannelli JR, Martin GR, Kleinman HK, Enhanced tumor growth of both primary and established human and murine tumor cells in athymic mice after coinjection with Matrigel, J. Natl. Cancer Inst 83 (1991) 769–774. [PubMed: 1789823]

[50]. Yamamura K, Kibbey MC, Jun SH, Kleinman HK, Effect of Matrigel and laminin peptide YIGSR on tumor growth and metastasis, Semin. Cancer Biol 4 (1993) 259–265. [PubMed: 8400148]

[51]. Uemura M, Refaat MM, Shinoyama M, Hayashi H, Hashimoto N, Takahashi J, Matrigel supports survival and neuronal differentiation of grafted embryonic stem cell-derived neural precursor cells, J. Neurosci. Res 88 (2010) 542–551. [PubMed: 19774667]

[52]. Wang J, Chu R, Ni N, Nan G, The effect of Matrigel as scaffold material for neural stem cell transplantation for treating spinal cord injury, Sci. Rep 10 (2020) 2576. [PubMed: 32054865]

[53]. Carlson BL, Pokorny JL, Schroeder MA, Sarkaria JN, Establishment, maintenance and *in vitro* and *in vivo* applications of primary human glioblastoma multiforme (GBM) xenograft models for translational biology studies and drug discovery, Curr. Protocol. Pharmacol 14 (2011). ChapterUnit 14 16.

[54]. Guastella AR, Michelhaugh SK, Klinger NV, Kupsky WJ, Polin LA, Muzik O, Juhasz C, Mittal S, Tryptophan PET imaging of the kynurenine pathway in patient-derived xenograft models of glioblastoma, Mol. Imaging 15 (2016).

[55]. Tsoli M, Shen H, Mayoh C, Franshaw L, Ehteda A, Upton D, Carvalho D, Vinci M, Meel MH, van Vuurden D, Plessier A, Castel D, Drissi R, Farrell M, Cryan J, Crimmins D, Caird J, Pears J, Francis S, Ludlow LEA, Carai A, Mastronuzzi A, Liu B, Hansford J, Gottardo N, Hassall T, Kirby M, Fouladi M, Hawkins C, Monje M, Grill J, Jones C, Hulleman E, Ziegler DS, International experience in the development of patient-derived xenograft models of diffuse intrinsic pontine glioma, J. Neurooncol 141 (2019) 253–263. [PubMed: 30446898]

[56]. Das A, Henderson F Jr., Lowe S, Wallace G C t, Vandergrift WA 3rd, Lindhorst SM, Varma AK, Infinger LK, Giglio P, Banik NL, Patel SJ, Cachia D, Single agent efficacy of the HDAC inhibitor DATS in preclinical models of glioblastoma, Cancer Chemother. Pharmacol 82 (2018) 945–952. [PubMed: 30209569]

[57]. Xue W, Ton H, Zhang J, Xie T, Chen X, Zhou B, Guo Y, Fang J, Wang S, Zhang W, Patient-derived orthotopic xenograft glioma models fail to replicate the magnetic resonance imaging features of the original patient tumor, Oncol. Rep 43 (2020) 1619–1629. [PubMed: 32323818]

[58]. Rajcevic U, Petersen K, Knol JC, Loos M, Bougnaud S, Klychnikov O, Li KW, Pham TV, Wang J, Miletic H, Peng Z, Bjerkvig R, Jimenez CR, Niclou SP, iTRAQ-based proteomics profiling reveals increased metabolic activity and cellular cross-talk in angiogenic compared with invasive glioblastoma phenotype, Mol. Cell. Proteomic 8 (2009) 2595–2612.

[59]. Sakariassen PO, Prestegarden L, Wang J, Skaftnesmo KO, Mahesparan R, Molthoff C, Sminia P, Sundlisaeter E, Misra A, Tysnes BB, Chekenya M, Peters H, Lende G, Kalland KH, Oyan AM, Petersen K, Jonassen I, Kogel van der A, Feuerstein BG, Terzis AJ, Bjerkvig R, Enger PO, Angiogenesis-independent tumor growth mediated by stem-like cancer cells, Proc. Natl. Acad. Sci. U.S.A 103 (2006) 16466–16471. [PubMed: 17056721]

[60]. Thorsen F, Jirak D, Wang J, Sykova E, Bjerkvig R, Enger PO, van der Kogel A, Hajek M, Two distinct tumor phenotypes isolated from glioblastomas show different MRS characteristics, NMR Biomed 21 (2008) 830–838. [PubMed: 18613001]

[61]. Ribatti D, The crucial role of vascular permeability factor/vascular endothelial growth factor in angiogenesis: a historical review, Br. J. Haematol 128 (2005) 303–309. [PubMed: 15667531]

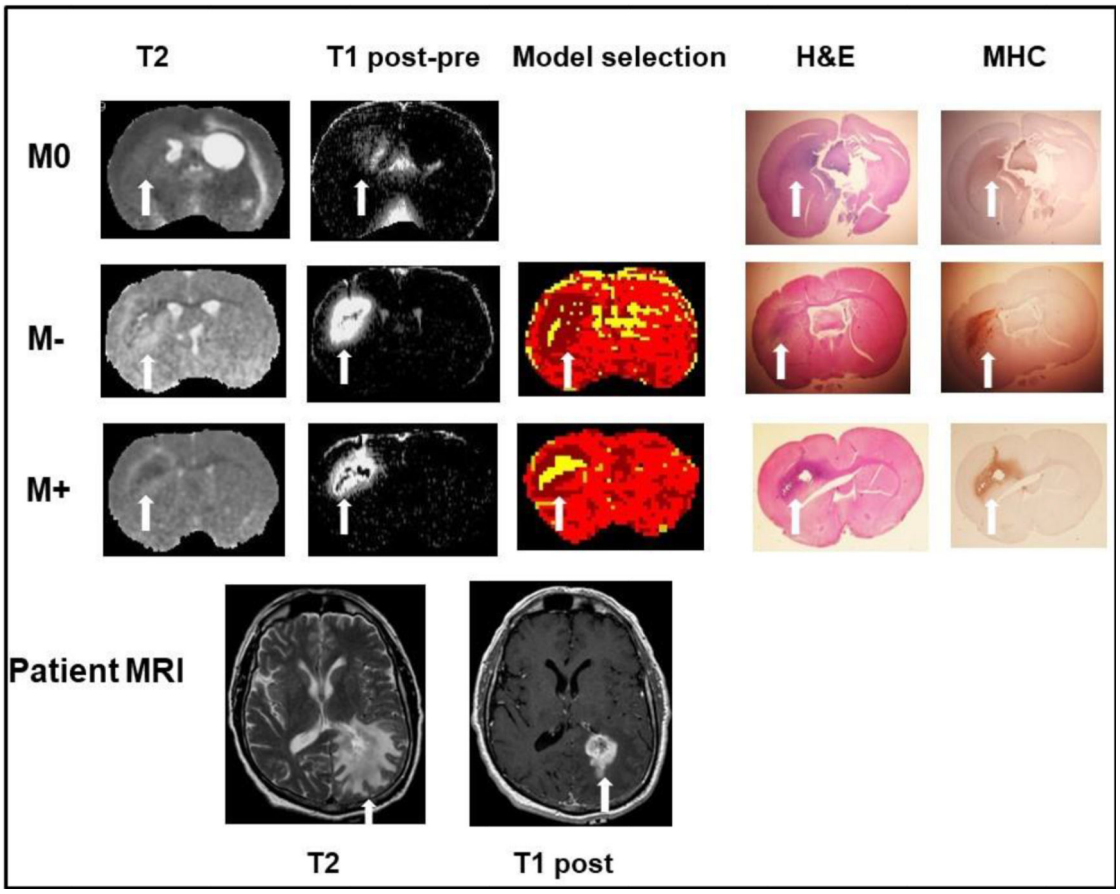

Fig. 1.

A collage of MRI and histology images from three HF3016 studies, one each from M0, M− and *M*+ groups along with their associated patient MRI images in the bottom panel. The embedded tumor is indicated by a solid, white arrow. Note the agreement between MRI and histology in tumor location, extent and central necrosis when present, in all cases. All three experimental groups showed T2 hyperintensity, but only M− and *M*+ groups showed T1-weighed contrast enhancement and could be used to produce maps of model selection. The H&E and MHCs-stained sections showed the contrast-enhancing tumor part, as well as the MRI-invisible, infiltrative tumor along white matter. The patient tumor showed both T2 hyperintensity and T1 contrast enhancements (bottom panel). The large T2 contrast enhancement in M0 is the enlarged, contralateral ventricle.

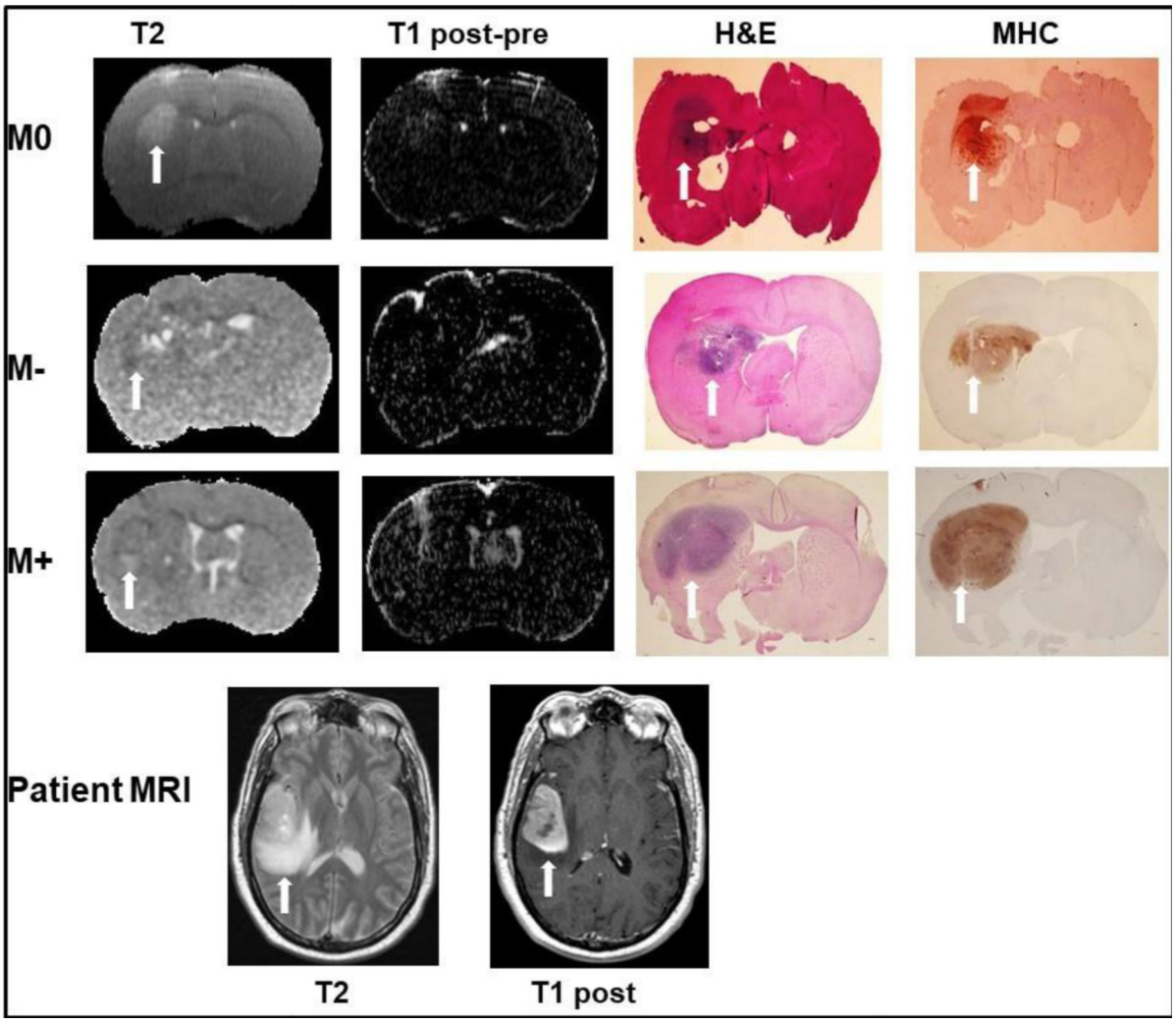

Fig. 2.

A collage of MRI and histology images from three HF2303 studies, one each from M0, M− and *M*+ groups along with their associated patient MRI images in the bottom panel. The embedded tumor, when visible, is indicated by a solid, white arrow. Note the agreement between MRI and histology in tumor location and extent. All three showed T2 hyperintensity, but none showed T1-weighed contrast enhancement. The H&E and MHCs-stained sections showed embedded as well as infiltrative tumor tissue. Note the small tumor segment on the cortical surface that showed T1 enhancement in all three experimental groups. Similar to the HF3016, HF2303 human tumor also showed both T2 hyperintensity and T1 contrast enhancements (bottom panel).

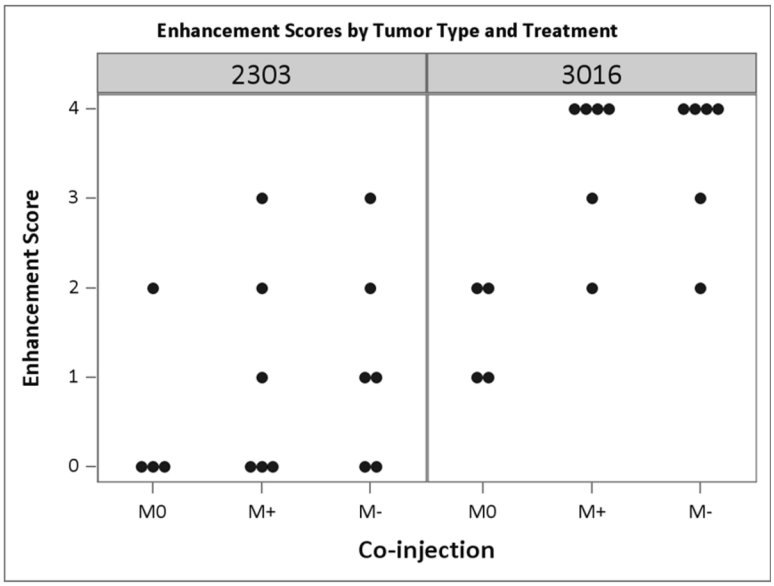

Fig. 3.

Dot plot of blinded scores from a neuroradiologist's assessment of T1-weighted contrast enhancement in the two tumor types. More rats in the HF3016 cohort were scored toward 4, florid enhancement.

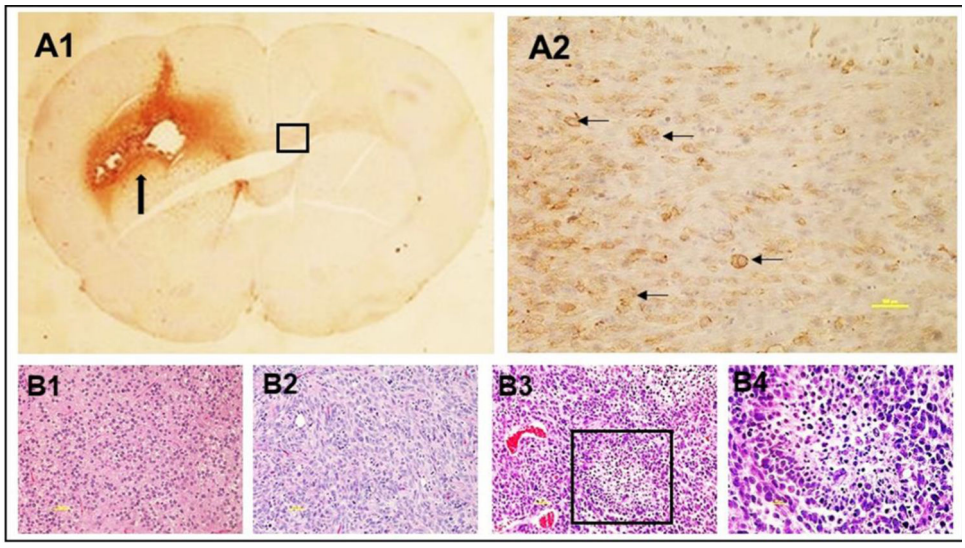

Fig. 4.

A1, MHC-stained coronal brain section (main tumor mass is indicated by a black solid arrow; also showed in Fig. 1); A2, box in A1 enlarged to show infiltrating glioma cells along the white matter, but invisible on MRI (some tumor cells are indicated by black arrows). B1 to B4 depict H&E-stained coronal brain sections from the two cell lines as described below to show microscopic, histopathologic features. B1, HF2303 M−; B2, HF3016 M0; B3, HF3016 M−; B4, box in B3 enlarged. Note the nearly uniform distribution of glioma cells in both B1 and B2 in comparison to regions with necrosis and irregular blood vessels in B3. B4 shows a region with pseudopalisading necrosis typical of GBM.

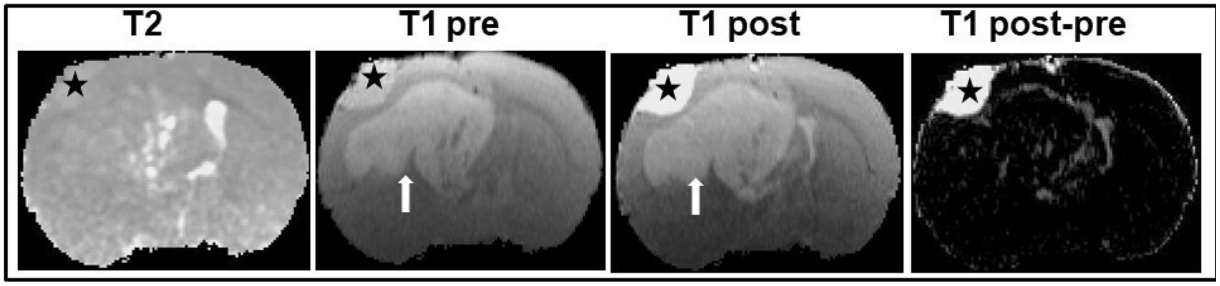

Fig. 5.

As in Figures 1 and 2, a typical set of images from an animal implanted with cell line HF2303, with co-injection of M+. There is florid T1 contrast enhancement of the extra-axial (black star), but not of the intra-axial tumor (solid white arrow).

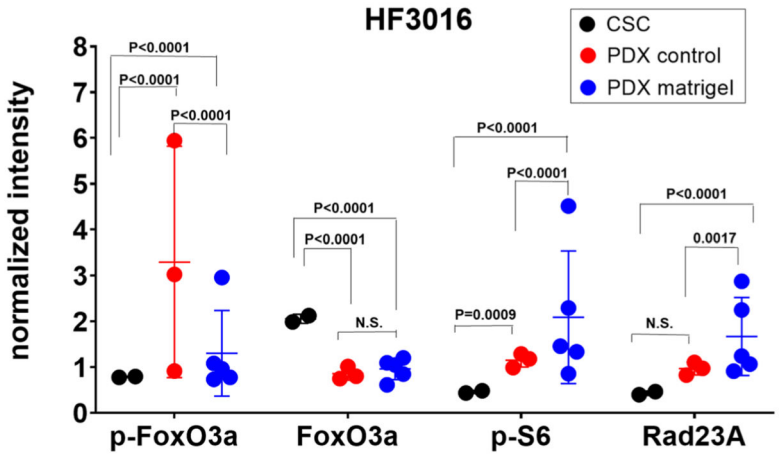

Fig. 6.

Long term effect of Matrigel at implant on the proteomic composition of rat HF3016 models. Normalized protein and phosphoprotein levels in the CSCs (n=2), PDOX tumors with no-matrigel control ($n = 3$), or with Matrigel ($n = 5$), measured by reverse-phase protein arrays (RPPA) and compared among groups using Holm-Sidak test. p-values are shown; N.S., non-significant.

Table 1

Tumor transvascular kinetics values for Magnevist in HF3016 M− and *M*+ tumors.

HF3016 M−	v_p	K^{trans}	v_e	V_D
Mean	0.0094	0.0386	0.1815	0.1651
SD	0.0062	0.0152	0.0479	0.0137
HF3016 *M*+	v_p	K^{trans}	v_e	V_D
Mean	0.0126[1]	0.0482[2]	0.3503[3]	0.2710[4]
SD	0.0050	0.0312	0.2175	0.1155

p values:

[1]0.49.

[2]0.56.

[3]0.12.

[4]0.08.